


Article

Microstructural Evolution and Mechanical Properties of Graphene-Reinforced Ti-6Al-4V Composites Synthesized via Spark Plasma Sintering

Wei Wang ^{1,*} , Haixiong Zhou ¹, Qingjuan Wang ^{1,*}, Baojia Wei ², Shewei Xin ³ and Yuan Gao ¹¹ School of Metallurgy Engineering, Xi'an University of Architecture and Technology, Xi'an 710055, China; haixiong@live.xauat.edu.cn (H.Z.); yuan-gao@foxmail.com (Y.G.)² School of Materials Science and Engineering, Northeastern University, Shenyang 110819, China; weibaojia@yeah.net³ Titanium Alloy Institute, Northwest Institute for Nonferrous Metal Research, Xi'an 710016, China; nwpu_xsw@126.com

* Correspondence: gackmol@163.com (W.W.); jiandawqj@163.com (Q.W.); Tel.: +86-029-8220-5097 (W.W. & Q.W.)

Received: 22 April 2020; Accepted: 27 May 2020; Published: 2 June 2020



Abstract: Ti-6Al-4V alloy (TC4) with different concentrations of graphene nanoplatelets (GNPs) were fabricated by ball milling and spark plasma sintering (SPS). Microstructure characteristics of the composites were characterized by X-Ray Diffraction (XRD), Scanning electron microscopy (SEM), and Raman. Microhardness and the compressive mechanical properties were also investigated. Experimental results showed that in the process of SPS, most of the GNPs were still retained at high pressure and temperature, and a new phase of TiC was presented due to the in-situ reaction between TiC and GNPs. Also, the strength of the composites was depended on the concentration of GNPs in TC4 matrix. Consequently, the composite with 0.8 wt. % GNPs was increased 18% in microhardness. The maximum yield strength and ductility of the composite were increased by 22.2% and 43.2%, respectively. The strengthening mechanism of the composites was further discussed, and the Orowan strengthening mechanism was the main strengthening factor.

Keywords: graphene nanoplatelets; metal-matrix composite; microstructure; mechanical properties; strengthening mechanism

1. Introduction

In recent years, graphene has become an ideal reinforcement in composites, because of its remarkable thermal, electrical and mechanical properties [1,2]. Graphene nanoplatelets (GNPs) have many merits such as lower price, easier to produce [3]. In current researches, GNPs have been investigated as a reinforcement in ceramic, polymeric and metallic matrix [3–5]. Considerable researches on graphene reinforced metal matrix composites have been conducted on the metal matrixes of copper [6–8], aluminum [9–11], magnesium [12,13]. In the investigations, the mechanical properties and tribological properties of the composites could be increased by the addition of GNPs [14,15].

Titanium alloys are mainly used in aerospace, medical apparatus and instruments and automotive because of their outstanding specific strength and corrosion resistance and excellent bio-compatibility [16–18]. In order to meet the increasing demand of light-weight structural materials, a lot of studies related to titanium matrix composites reinforced by different reinforced phases such as TiB [19], TiC [20], carbon nanotubes [21] and SiC fibers [22] were conducted using various methods. Compared with these reinforced phases, GNPs have better the fracture strength, Young's modulus, the aspect ratio and specific surface [23–25]. Therefore, some research work have been carried out in the titanium matrix composite reinforced by GNPs. Liu et al. [23] prepared the graphene/ titanium (Ti)

composites through spark plasma sintering (SPS) and reported that graphene/titanium (Ti) composites have great improvement of the yield strength and compressive strength. Mu et al. [24,25] researched the microstructure, interface evolution and tensile properties of pure titanium based composites with graphene nanosheets fabricated by ball milling dispersion, SPS sintering and subsequently hot-rolling, and found that graphene was retained in the composites, the interface characteristics of TiC and the ultimate tensile strength of composites with merely 0.1 wt. % GNPs addition has increased by 54.2% compared with pure titanium. Zhou et al. [26] found that TiAl based composites with the addition of graphene have better wear resistance and tensile strength. Thus, the use of GNPs as a reinforcing phase could improve the mechanical properties of titanium alloy. Ti6Al4V alloy as the common commercial titanium alloys have a wide range of applications. However, so far, there is little information available on the effects of GNPs on the strengthening mechanism of the GNPs/Ti6Al4V composites prepared by SPS method [27].

Therefore, in the present investigation, Ti6Al4V matrix composites with few-layer GNPs were fabricated via mechanically ball-milling (BM) and then SPS sintering. The microhardness and compressive performances at room and high temperature of the GNPs/Ti6Al4V composite were investigated. Mechanical behavior of the composites was analyzed in terms of the microstructural features. The strengthening mechanisms of the composites were discussed by two main strengthening factors combined with the modified load transfer model and the modified fine-grain strengthening model.

2. Experimental Procedure

2.1. Raw Materials

Ti6Al4V pre-alloy powders (Sino-Euro Materials Technologies of Xi'an Co., Ltd., Xi'an, China) with density 4.51 g/cm^3 as the source of raw materials were used in this investigation. It contains 6.21 wt. % Al, 3.95 wt. % V, 0.20 wt. % Fe, 0.01 wt. % N and balance Ti. Scanning electron microscopy (SEM) (Hitachi SU 3500, Tokyo, Japan) images of these powders were showed in Figure 1a. It found that the average particle size of these spherical powders were $85 \mu\text{m}$. The microstructure of TC4 pre-alloy powders consists mainly of α -Ti and β -Ti phase (Figure 1b). Powders of GNPs as the raw material were provided from Hunan Jinyang Carbon New Materials Co., Ltd., Changsha, China. From the SEM image of GNPs, wrinkles and folds can be found (Figure 1c). Raman (chem200, Sciaps, Boston, MA, USA) analysis was adopted to investigate the structure of GNPs (Figure 1d), the 2D peak intensity is significantly lower than the G peak, indicating that the multilayer GNPs were used in this experiment.

2.2. Preparation Process of the Composites

The preparation processes of the GNPs/TC4 composite were mainly contained two steps (I)–(II) in Figure 2.

- (I) Preparation of the composite powders. The different contents of GNPs were mixed with TC4 pre-alloyed powders by using a low energy ball mill (QM-3SP2, Nanda instrument plant, Nanjing, China) with the speed of 300 rpm for 16 h under Ar atmosphere. The mixed powders were put into a zirconia ceramics vial with the zirconia ceramics balls. The diameters of the stainless steel balls are 10 mm and 6 mm, respectively. The weight ratio of the large ball and the small ball was 1:1. The weight ratio of the mixed powder and the ball was 1:10. Identification code of each composite prepared in this work is the followings, Ti6Al4V-Graphene (TG), TG0.2, TG0.4, TG0.6, and TG0.8 is assigned to the composites with 0–0.8 wt. % of GNPs, respectively.
- (II) Sintering of the composite powders. Five mixed powders (TG, TG0.2, TG0.4, TG0.6, and TG0.8) were sintered by SPS machine (labox-1575, sinter land, Nagaoka, Japan). Firstly, the mixed powders were filled into the graphite mold, and then two graphite punches were pressed on the powders. The GNPs/TC4 composites were fabricated for 40min at 1200°C with a heating rate of 100°C , under unit pressure of 50 MPa. After sintering, the sintered compact was cooled to the

room temperature (RT) in the furnace. Finally, the sintered composites of $\varnothing 20 \text{ mm} \times 12 \text{ mm}$ were obtained (Figure 2).

2.3. Microstructure Characterization and Mechanical Properties Testing

The sintered samples were cut using an electrospark wire-electrode cutting system and were prepared by standard mechanical grinding and polishing. The samples were etched using a Kroll solution (1 mL HF:3 mL HNO₃:10 mL H₂O) after mechanical polishing. The microstructure characteristics of the mixed powders and composites were characterized by X-Ray Diffraction (XRD) (D8 advance, Bruker Axs, Karlsruhe, Germany), SEM (zeiss G300, Oberkochen, Germany) and Raman spectroscopy (Chem200, Sciaps, Boston, MA, USA). Microhardness of the composites was evaluated with a load of 3 N for 10 s by the digital micro-hardness tester (HV-1000, Guangdong, China). Average micro-hardness was acquired by nine sets of data points. Sample size of $\varnothing 6 \text{ mm} \times 9 \text{ mm}$ were used for compression tests at room temperature and 800 °C. The whole test process was performed on a thermal simulation machine (Gleeble 3800, DSI, MN, USA) at a constant beam moving speed of 0.54 mm/min.

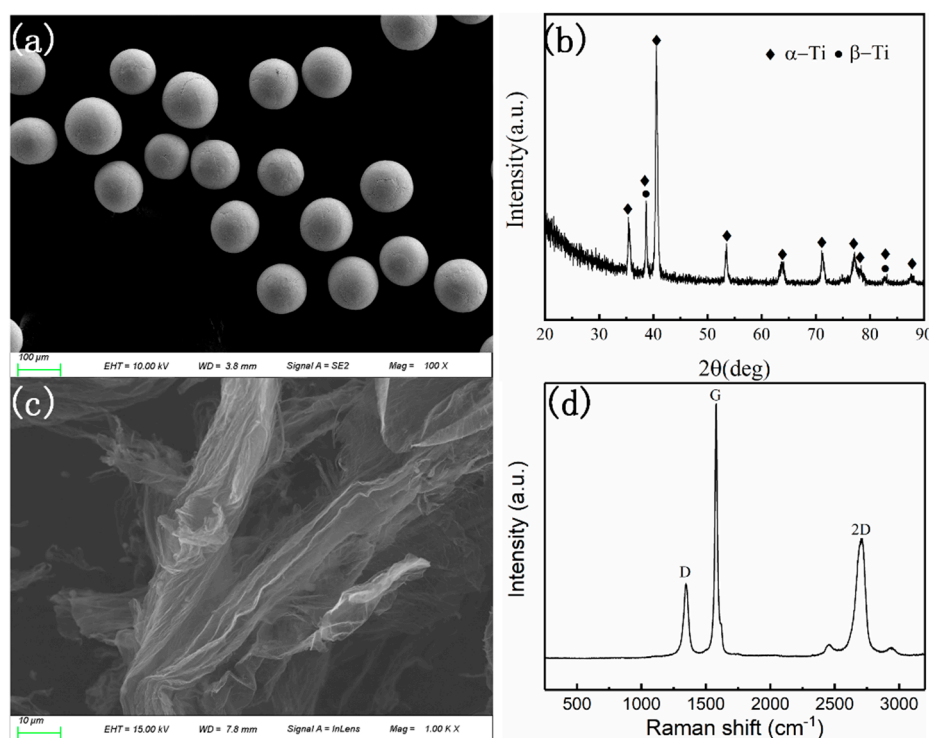


Figure 1. (a) Scanning electron microscopy (SEM) micrograph of the TC4 pre-alloy; (b) X-Ray Diffraction (XRD) patterns of the TC4 pre-alloy; (c) SEM micrograph of the Graphene nanoplatelets (GNPs); (d) Raman spectrum of the GNPs.

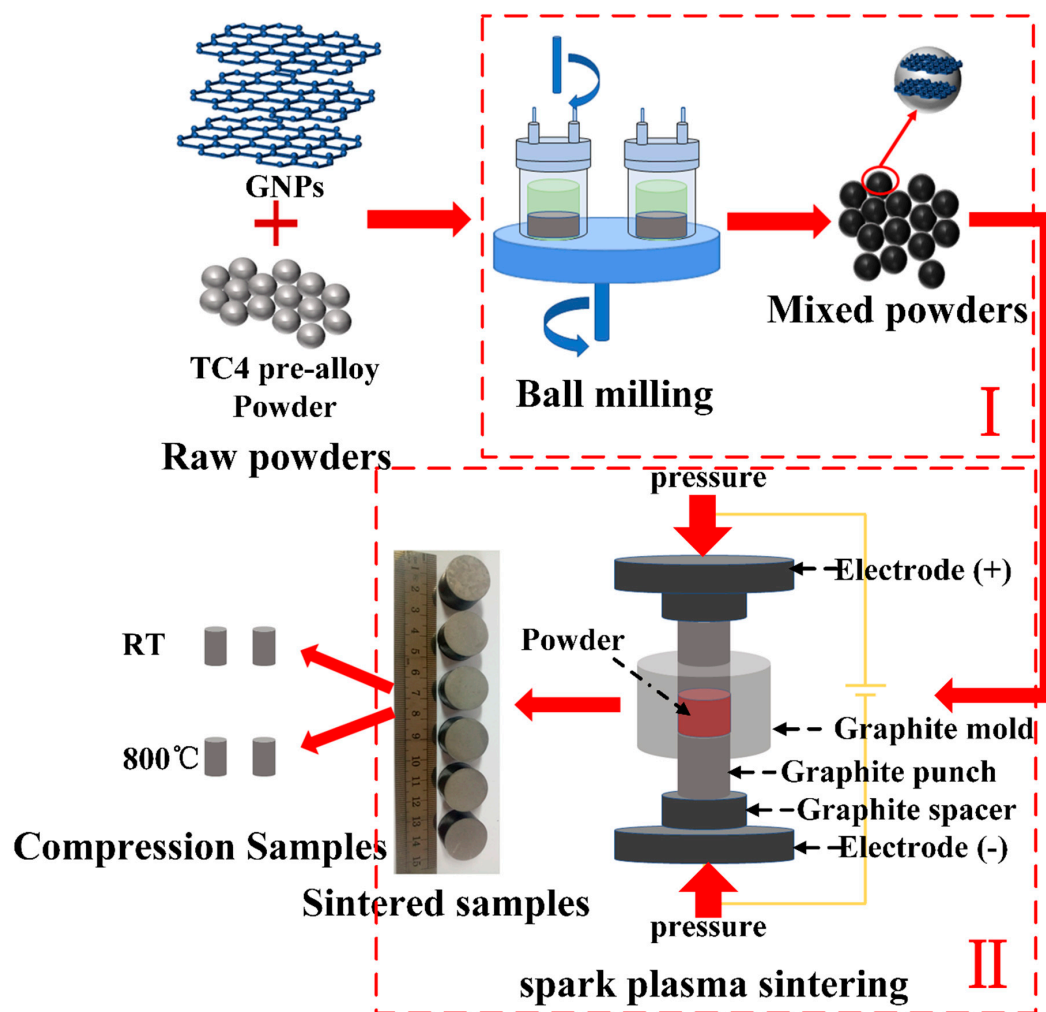


Figure 2. Preparation processes of GNPs/TC4 composite.

3. Results and Discussion

3.1. Microstructures of the Mixed Powders

From XRD results of the mixed powders (Figure 3a), it can be seen that the diffraction peaks of α -Ti and β -Ti phase were presented in the powders of raw materials. Figure 3b–d show SEM images of the mixed powders. Compared with TC4 pre-alloyed powders, GNPs were adsorbed on the surface of TC4 particles. As the GNPs of the composites increased, more and more GNPs were detected on the surface of the mixed powders. After low energy ball mill, the GNPs were distributed uniformly on the surface of the Ti6Al4V pre-alloy powders (Figure 3e).

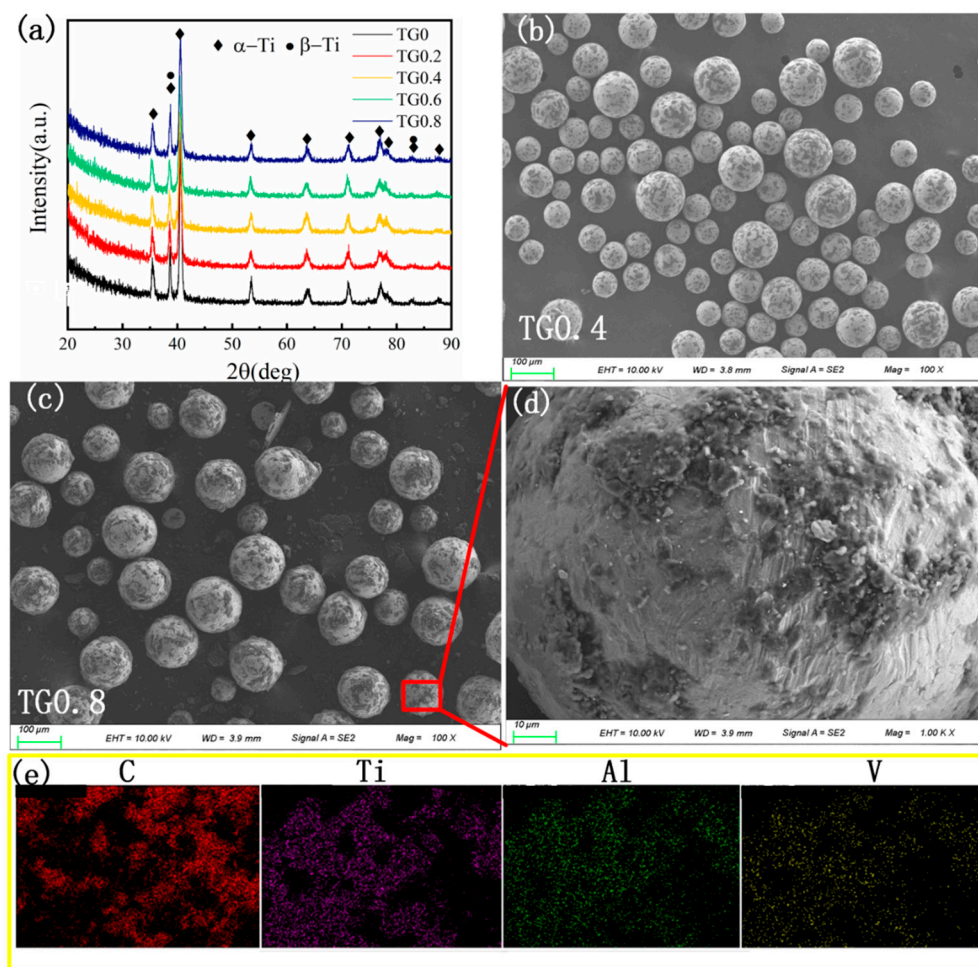


Figure 3. (a) XRD patterns of GNP/TC4 mixture powders; (b) SEM images of TG0.4 mixture powders; (c) SEM images of TG0.8 mixture powders; (d) an enlarged view of red rectangle position marked in (c); (e) Energy disperse spectroscopy (EDS) mapping results in (d).

3.2. Microstructure of the Sintered GNP/TC4 Composites

XRD images of the sintered GNP/TC4 samples are showed in Figure 4a. Compared with these mixed powders, the peaks of α and β phase were also emerged in the GNP/TC4 composites. From the XRD diffraction patterns, the diffraction peaks of graphene were still not detected, while the new phase TiC was formed. It is because that the content of GNPs in the composites are very low. On the other hand, due to the obvious difference between the mass absorption coefficient of titanium ($208 \text{ m}^2/\text{g}$) and carbon ($4.6 \text{ m}^2/\text{g}$), it lead to the absence of the XRD pattern peaks of GNPs [24]. As the concentration of GNPs increased, the XRD intensities of TiC were further increased. Moreover, the diffraction peaks of the composites were broadened [25]. The main reason is that GNPs and in-situ TiC dispersions could effectively restrain grain growth. From Raman spectra, the characteristic peaks of D (1355 cm^{-1}), G (1580 cm^{-1}) and 2D (2700 cm^{-1}) bands were presented. The intensity of the 2D band is significantly lower than that of G band. The relative intensity between D peaks and G peaks (I_D/I_G) indicated that the structural defects of GNPs were detected in the composites [26–29]. Compared with TC4 alloy prepared by SPS technique, the I_D/I_G ratio of the composite with 0.4 wt. % GNPs was increased significantly from 0.30 to 0.46. It is indicated that the structure of the GNPs was destroyed in ball milling and sintering process. As the content of GNPs increased to 0.8 wt. % in the composites, the I_D/I_G ratio (~ 0.45) was similar to the composites with the GNPs of 0.4 wt. %. It means that ball milling and sintering process is the most important factors that affect the I_D/I_G ratio of composites.

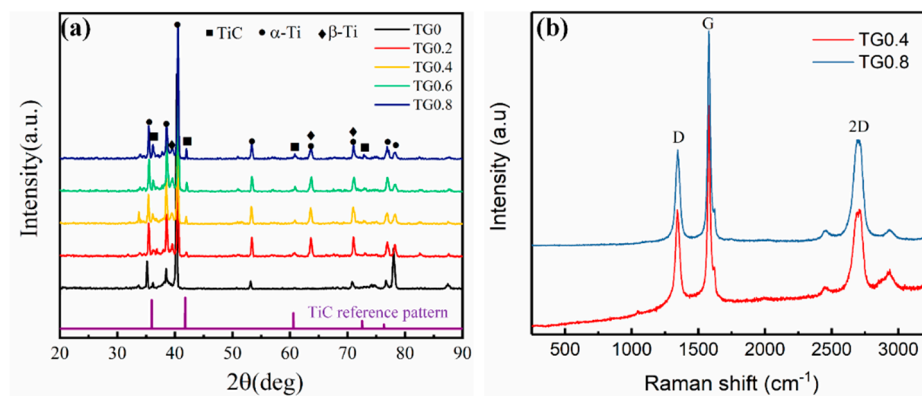


Figure 4. GNPs/TC4 composites sintered (a) XRD patterns (b) Raman spectra.

In SEM images of Figure 5a–e, it can be observed that many particles were presented on the grain boundaries of the composites. The Energy disperse spectroscopy (EDS) results showed that in the region of the grain boundary, there are abrupt changes in the distribution of carbon and alloy elements (Figure 5f). According to the EDS and Raman spectrum analysis, it concluded that GNPs were also retained on the grain boundary. Beyond that, the elemental composition of the gray region on the grain boundaries is approximately 49.35% Ti, 1.67% Al, 1.23%V and 47.75% C. The gray region was mainly consisted of Ti and C and the atomic ratio of Ti/C is nearly 1:1. Therefore, the gray region should be TiC, which is consistent with the XRD results. This indicates that the TiC particles were formed by the reaction of the GNPs and Ti matrix. In the composites of TG0.2 and TG0.4, GNPs and TiC were discontinuous at the grain boundary. As the concentration of the GNPs was further increased (TG0.6 and TG0.8), GNP and TiC were continuous at the grain boundary. From the SEM image of the GNPs/TC4 composite, it can be observed that the GNPs/TC4 composites presented a finer microstructure. In the GNPs/TC4 composite, the grain sizes were significantly reduced with increasement of the concentration of GNPs. Due to the pinning effect of the GNPs and TiC at the grain boundaries, the composites have smaller grain size.

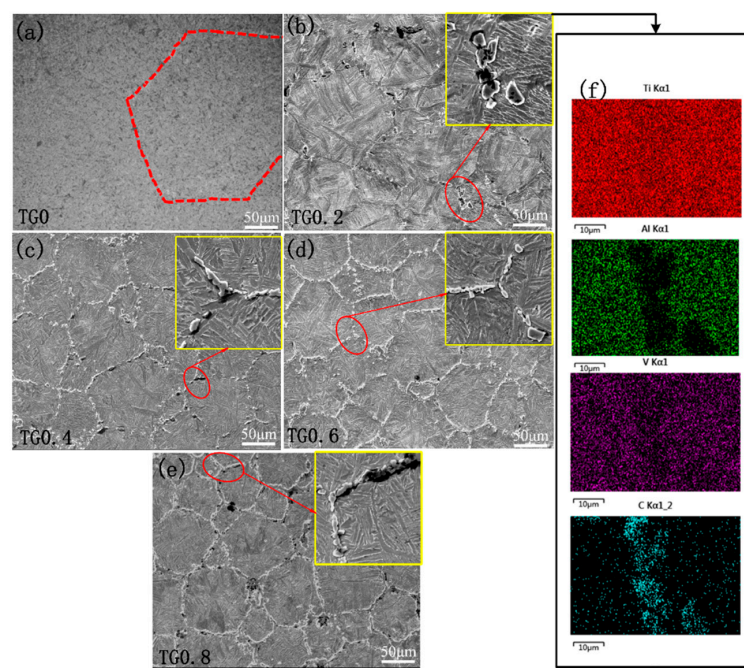


Figure 5. SEM images of composites prepared (a) TG0; (b) TG0.2; (c) TG0.4; (d) TG0.6; (e) TG0.8 and (f) an EDS mapping of yellow rectangle position marked in (b).

3.3. Mechanical Properties

The average microhardness of the composites is shown in Figure 6. As the concentration of the GNPs of the composites increased, the average microhardness of the composites was also increased. Compare with pure TC4 alloy, the average microhardness of the composites of TG0.8 was increased by 18 percent. The compressive properties of the composites are showed in Figure 7. In pure TC4 alloy, the fracture strength of 1132 ± 17 MPa and compressive strain of 23% were obtained. As the contents of GNPs in the composites increased, the strength and compressive strain were also increased. As the content of GNPs increased to 0.8 wt. %, the highest fracture strength of 1443 ± 12 MPa and compressive strain of 21.6% were obtained. The yield stress of pure TC4 alloy is only 941 ± 13 MPa, while the composite with 0.2 wt. % GNPs could be increased to 1052 ± 12 MPa. As the concentration of GNPs increased, the yield stress was gradually increased. When the contents of GNPs increased to 0.8 wt. %, the yield stress of the composite was increased to 1209 ± 15 MPa, and an increase of ductility was about 22.2%. The compressive strain of pure TC4 alloy is only 22.6%, while it was increased to about 39.8% when adding the GNPs of 0.2 wt. %, and an increase of the ductility was about 43.2%. When the concentration of the GNPs increased to 0.8 wt. %, the compressive strain was decreased. However, the compressive strain in this composite is still higher than that of pure TC4 alloy. Figure 7b shows the engineering stress-engineering strain curves of the composites at the temperature of 800 °C. The compressive strength of pure TC4 ally at 800 °C was 121 MPa, as the concentrations of GNPs increased, the compressive strengths of the composites were also increased gradually. The compressive strength of the composites of TG0.8 was 221.5 MPa, which was 45.3% higher than that of pure TC4. However, from the image of the engineering stress-engineering strain curve of the composite of TG0.8, the flow stress was decreased rapidly after reaching the maximum. It means that the ductility of this composite was poor. When the concentration of GNPs was less than 0.8 wt. %, the flow stress at high-temperature compression curve was not decreased significantly, and the cracks are not generated on the surface of the compressed samples. It indicated that the composites containing GNPs less than 0.6 wt. % have good ductility.

From the above analysis, GNPs have an effective reinforcement in the TC4 alloy. In this experiment, it was also found that GNPs is benefit for improving the ductility of the composites. In previous investigations, few research results could improve strength and ductility of the GNPs /titanium composites. Yan et al [30] showed that graphene nanoflakes reinforced aluminum alloy matrix composites achieved a remarkable enhancement of strength and ductility. Xiong et al. [31] showed that the yield strength (233 ± 15 MPa) and ductility of graphene-copper composites were improved. The key toughening mechanisms of the graphene reinforced metal matrix composites can be summarized as follows. First of all, the remarkable ductility of the composites could be attributed to the multiply wrinkled structure of the GNPs (Figure 1c). On the other hand, the energy consumption of the crack migration process increases the toughness of the material. When a crack appears under the stress of the material, the initial crack will tilt and twist when it encounters the graphene and the in-situ TiC crack generated, forcing it to leave the initial extension surface. Due to the discontinuous distribution of graphene and TiC, the crack encountered more obstacles during development. The deflection of the crack increases the resistance of crack propagation and improves the ductility of the composites [30,31].

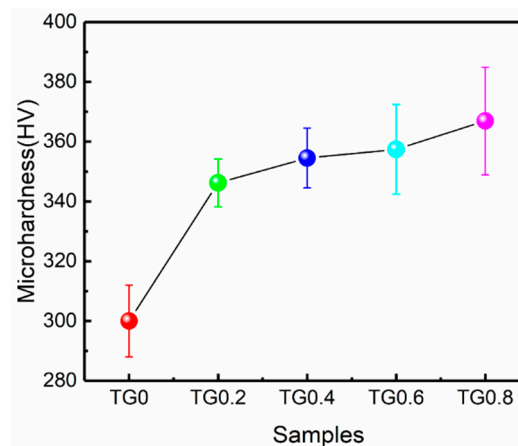


Figure 6. Microhardness of the pure TC4 alloy and the composite with different concentration of the GNPs.

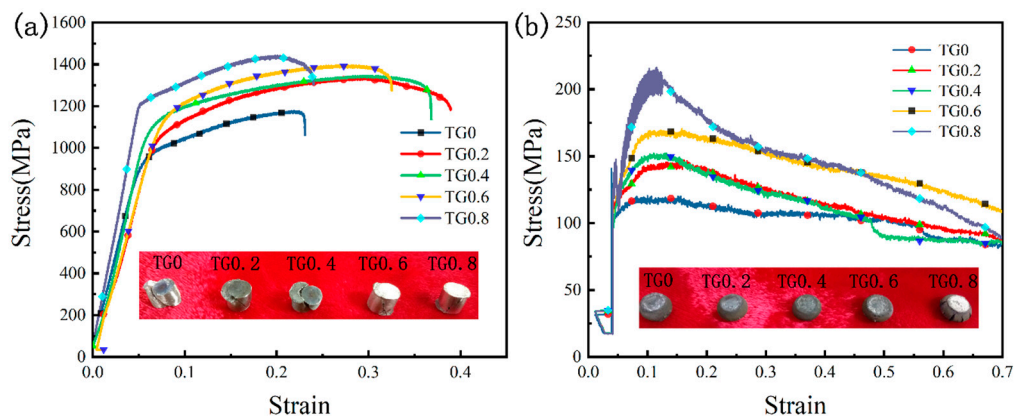


Figure 7. Engineering stress–engineering strain curves of the GNPs/TC4 composites from the compress test (a) RT; (b) 800 °C.

The rule of mixture makes a simplified model for estimating the mechanical properties of the composites [32,33]. Since it is impossible to measure the content of in-situ TiC generated by GNPs, which one of GNPs and TiC have an important role for improving the strength of the composite materials. Therefore, the mixing law was used to calculate GNPs ($a = 1$, $b = 0$) and TiC ($a = 0$, $b = 1$). In this model, the theoretical value of the yield strength can be expressed as:

$$\sigma_{TG} = (1 - f_V)\sigma_T + f_V(a\sigma_G + b\sigma_C) \quad (1)$$

where σ_{TG} is yield strength of the GNPs/TC4 composite as calculated from the mixing rules, f_V is the volume fraction of GNPs, σ_T is the yield strength of the TC4 matrix (941 MPa in this work), σ_G ($\sigma_G = 30$ GPa) is the yield strength of reinforcement (GNPs) and σ_C ($\sigma_C = 4$ GPa) is the yield strength of reinforcement (TiC) [14,20]. The results calculated by the mixing model are shown in Figure 8a. It can be observed that the results calculated by the rule of mixture with GNPs as the reinforcing phase are consistent with our experimental results. Namely, although TiC was generated in the composites, but GNPs strengthening had a leading role in GNPs/TC4 composites.

GNPs and in-situ TiC are discontinuously distributed in the TC4 matrix, they could prevent the path of dislocations. Through the analysis of mechanical properties of composites, it can be found that GNPs could significantly improve the mechanical strength of the material. Further analysis of the strengthening mechanism of GNPs-added composites. There are four main models for the strengthening mechanism, namely shear lag strengthening mechanism [34,35], thermal mismatch strengthening mechanism [36,37], Orowan strengthening mechanism [38,39] and fine grain

strengthening mechanism [40,41]. The main dominant mechanism of GNPs reinforced metal matrix composites is generally shear lag strengthening mechanism and Orowan strengthening mechanism. Therefore, the shear strength and Orowan strengthening model were chosen to verify the dominant enhancement mechanism of this study.

- (1) The shear lag model [36] is an important model to explain the strengthening mechanism. Addition of GNPs are beneficial for transferring of the load from the matrix to the GNPs and the in-situ TiC, but the interfacial shear stress was produced during the stress transfer process. Thus, the interfacial bond affects the strength of the composite. The result of this work increasing the strength of the composite. Based on the shear lag model, yield strength of the GNPs/TC4 composite can be expressed using:

$$\sigma_{SL} = \left(1 + \frac{f_V l}{2}\right) \sigma_T \quad (2)$$

where σ_{SL} is the yield strength calculated by shear lag model, f_V is volume fraction of GNPs, σ_T is the yield strength of the matrix and l is the aspect ratio of GNP.

- (2) Orowan strengthening is another strengthening mechanism of the GNP/TC4 composite compared to the monolithic TC4 alloy [38]. The addition of GNPs can improve the strength of the composites. The yield strength of the GNPs/TC4 composite based on the Orowan model, is showed as follows:

$$\sigma_{Oro} = \sigma_T \left(1 + \frac{1}{2} f_V\right) (1 + \sigma_C) (1 + \sigma_{OG}) \quad (3)$$

$$\sigma_C = \frac{1.25 G_T b}{\sigma_T} \sqrt{\frac{12(T_{process} - T_{test})(C_T - C_G) f_V}{b d_G (1 - f_V)}} \quad (4)$$

$$\sigma_{OG} = \frac{0.13 G_T b}{\sigma_T d_G \left[\left(\frac{1}{2 f_V}\right)^{1/3} - 1\right]} \ln \frac{d_G}{2b} \quad (5)$$

where σ_{Oro} is yield strength of GNPs-reinforced composite as calculated from Orowan strengthening mold, σ_T is the yield strength of the TC4 matrix under same processing conditions, f_V is volume fraction of GNPs, σ_C is increase in yield strength due to the thermal mismatch between the TC4 matrix and the reinforcement GNPs, σ_{OG} is increase in yield strength due to the Orowan strengthening effect, G_T is the shear modulus of the TC4 matrix, b is the magnitude of the Burgers vector of dislocations in TC4 matrix, $T_{process}$ ($T_{process} = 1200$ °C) is the processing temperature, T_{test} ($T_{test} = 20$ °C) is the test temperature, d_G means particle size of GNP, C_T ($C_T = 8.6 \times 10^{-6}$ °C⁻¹) and C_G ($C_G = 0.9 \times 10^{-6}$ °C⁻¹) are the coefficient of thermal expansion of the TC4 matrix and the reinforcement phase, respectively [14,42].

Based on the two strengthening model and current experimental data, the comparison and analysis are made on Figure 8b. The experimental data in the figure is the same as the curve of the data calculated by Orowan strengthening model, and their values are very close. The experimental data is not in accordance with the Orowan strengthening model data. It may be due to the fact that some GNPs reacts with the matrix to form TiC during the sintering process, which causes the experimental data to slightly deviate from the Orowan strengthening model data. This finding clearly indicates from the above discussion that the Orowan mechanism is the main strengthening mechanism in the GNPs-reinforced TC4 alloy. The discontinuous distribution of GNPs in the TC4 matrix effectively limits the movement of dislocations in the matrix, led to dislocation density increasing at the GNPs/TC4 interface [43]. Dislocation motion is the main mode of metal deformation. Therefore, it can be concluded that GNPs hinders dislocation motion as main strengthening mechanism in composite strength.

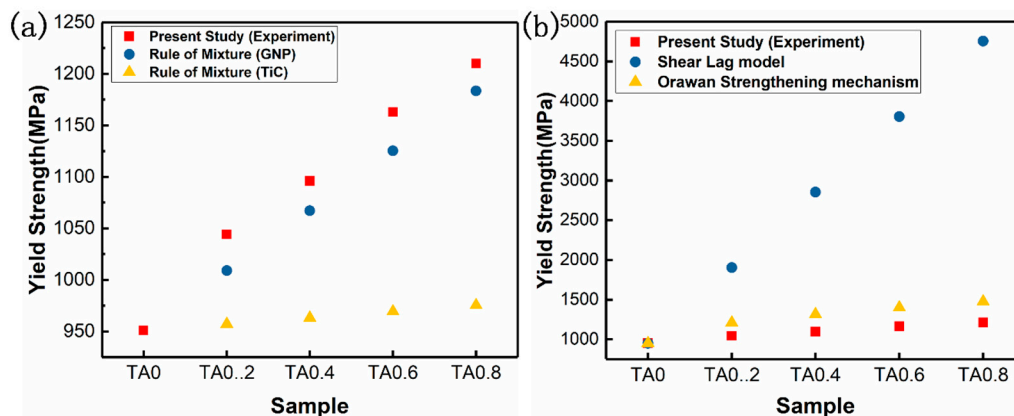


Figure 8. Comparison of yield strength calculated using different models and present study (a) Rule of mixture (b) Shear lag model and Orowan strengthening mechanism.

4. Conclusions

In this investigation, Ti6Al4V/GNPs composites were fabricated by ball milling and SPS. The microstructure, mechanical properties and strengthening mechanism of the composites were investigated. In the process of SPS, most of the GNPs were still retained at high pressure and temperature, and a new phase of TiC was presented due to the in-situ reaction between TiC and GNPs. As the contents of GNPs increased, the grain sizes of the composites were decreased due to the pinning effect of GNPs and in-situ TiC. The microhardness and compressive strength of the composites were increased after adding the GNPs into the Ti6Al4V alloy. Adding a small amount of GNPs can effectively improve the strength and ductility of the composites. Based on the experimental data and theoretical analysis, the Orowan mechanism is the main strengthening mechanism. Overall, our experimental results demonstrate that GNPs can actually act as an effective reinforcement in Ti6Al4V matrix composite materials. In addition, the present work provides valuable information that the potential for GNPs to be successfully used as a reinforcing phase in other metal matrix composite materials synthesized by SPS.

Author Contributions: Data curation, W.W., H.Z., B.W. and Y.G.; funding acquisition, W.W., Q.W. and S.X.; methodology, W.W., Q.W. and S.X.; supervision, Q.W. and S.X.; writing—original draft, H.Z. and Y.G.; writing—review and editing, W.W. All authors have read and agreed to the published version of the manuscript.

Funding: The current researched were supported by the fund of the National Natural Science Foundation of China (No. 51975450, 51605249), International Scientific and Technological Cooperation Program of the Shaanxi Province (No. 2019KW-026, 2019KW-064), Basic Project of Education Department of Shaanxi Province (No. 19JK0458), and Key Research and Development Program of Shaanxi (Program No.2018GY-119).

Acknowledgments: The authors thank Tao Xiong from the Shaanxi University of Science and Technology for performing the preparation of graphene-reinforced Ti-6Al-4V composites synthesized via spark plasma sintering.

Conflicts of Interest: The authors declare no conflict of interest.

References

- Novoselov, K.S.; Geim, A.K.; Morozov, S.V.; Jiang, D.; Zhang, Y.; Dubonos, S.V.; Grigorieva, I.V.; Firsov, A.A. Electric field effect in atomically thin films. *Science* **2004**, *306*, 666–669. [\[CrossRef\]](#)
- Schedin, F.; Geim, A.K.; Morozov, S.V.; Hill, E.W.; Blake, P.; Katsnelson, M.L.; Novoselov, K.S. Detection of individual gas molecules adsorbed on graphene. *Nat. Mater.* **2007**, *6*, 652–655. [\[CrossRef\]](#)
- Mu, X.N.; Cai, H.N.; Zhang, H.M.; Fan, Q.B.; Wang, F.C.; Zhang, Z.H.; Ge, Y.X.; Shi, R.; Wu, Y.; Wang, Z.; et al. Uniform dispersion and interface analysis of nickel coated graphene nanoflakes/pure titanium matrix composites. *Carbon* **2018**, *137*, 146–155. [\[CrossRef\]](#)
- Lee, C.; Wei, X.; Kysar, J.W.; Hone, J. Measurement of the elastic properties and intrinsic strength of monolayer graphene. *Science* **2008**, *321*, 385–388. [\[CrossRef\]](#)

5. Walker, L.S.; Marotto, V.R.; Rafiee, M.A.; Koratkar, N.; Corral, E.L. Toughening in graphene ceramic composites. *ACS Nano* **2011**, *5*, 3182–3190. [[CrossRef](#)]
6. Chen, F.Y.; Ying, J.M.; Wang, Y.F.; Du, S.Y.; Liu, Z.P.; Huang, Q. Effects of graphene content on the microstructure and properties of copper matrix composites. *Carbon* **2016**, *96*, 836–842. [[CrossRef](#)]
7. Zhang, D.; Zhan, Z.J. Preparation of graphene nanoplatelets-copper composites by a modified semi-powder method and their mechanical properties. *J. Alloy. Comp.* **2016**, *658*, 663–671. [[CrossRef](#)]
8. Jiang, R.; Zhou, X.; Fang, Q.; Liu, Z.P. Copper-graphene bulk composites with homogeneous graphene dispersion and enhanced mechanical properties. *Mater. Sci. Eng. A* **2016**, *654*, 124–130. [[CrossRef](#)]
9. Shin, S.E.; Bae, D.H. Deformation behavior of aluminum alloy matrix composites reinforced with few-layer graphene. *Compos. Part A* **2015**, *78*, 42–47. [[CrossRef](#)]
10. Asgharzadeh, H.; Sedigh, M. Synthesis and mechanical properties of Al matrix composites reinforced with few-layer graphene and graphene oxide. *J. Alloy. Comp.* **2017**, *728*, 47–62. [[CrossRef](#)]
11. Feng, S.W.; Guo, Q.; Li, Z.; Fan, G.L.; Li, Z.Q.; Xiong, D.B.; Su, Y.S.; Tan, Z.Q.; Zhang, J.; Zhang, D. Strengthening and toughening mechanisms in graphene-Al nanolaminated composite micro-pillars. *Acta Mater.* **2017**, *125*, 98–108. [[CrossRef](#)]
12. Xiang, S.L.; Gupta, M.; Wang, X.J.; Wang, L.D.; Hu, X.S.; Wu, K. Enhanced overall strength and ductility of magnesium matrix composites by low content of graphene nanoplatelets. *Compos. Part A* **2017**, *100*, 183–193. [[CrossRef](#)]
13. Du, X.; Du, W.B.; Wang, Z.H.; Liu, K.; Li, S.B. Ultra-high strengthening efficiency of graphene nanoplatelets reinforced magnesium matrix composites. *Mater. Sci. Eng. A* **2018**, *711*, 633–642. [[CrossRef](#)]
14. Bisht, A.; Srivastava, M.; Kumar, R.M.; Lahiri, I.; Lahiri, D. Strengthening mechanism in graphene nanoplatelets reinforced aluminum composite fabricated through spark plasma sintering. *Mater. Sci. Eng. A* **2017**, *695*, 20–28. [[CrossRef](#)]
15. Yang, Z.Y.; Wang, L.D.; Shi, Z.D.; Wang, M.; Cui, Y.; Wei, B.; Xu, S.C.; Zhu, Y.P.; Fei, W.D. Preparation mechanism of hierarchical layered structure of graphene/copper composite with ultrahigh tensile strength. *Carbon* **2018**, *127*, 329–339. [[CrossRef](#)]
16. Lütjering, G.; Williams, J.C.; Gysler, A. *Titanium Engineering Materials and Progresses*, 2nd ed.; Springer: Berlin, Germany, 2007.
17. Kondoh, K.; Threrujirapapong, T.; Umeda, J.; Fugetsu, B. High-temperature properties of extruded titanium composites fabricated from carbon nanotubes coated titanium powder by spark plasma sintering and hot extrusion. *Compos. Sci. Technol.* **2012**, *72*, 1291–1297. [[CrossRef](#)]
18. Wang, F.C.; Zhang, Z.H.; Sun, Y.J.; Liu, Y.; Hu, Z.Y.; Wang, H.; Korznikov, A.V.; Korznikova, E.; Liu, Z.F.; Osamu, S. Rapid and low temperature spark plasma sintering synthesis of novel carbon nanotube reinforced titanium matrix composites. *Carbon* **2015**, *95*, 396–407. [[CrossRef](#)]
19. Yan, Z.; Chen, F.; Cai, Y.; Zheng, Y. Microstructure and mechanical properties of insitu synthesized TiB whiskers reinforced titanium matrix composites by high-velocity compaction. *Powder Technol.* **2014**, *267*, 309–314. [[CrossRef](#)]
20. Luo, S.D.; Li, Q.; Tian, J.; Wang, C.; Yan, M.; Schaffer, G.B.; Qian, M. Self-assembled, aligned TiC nanoplatelet-reinforced titanium composites with outstanding compressive properties. *Scr. Mater.* **2013**, *69*, 29–32. [[CrossRef](#)]
21. Li, S.F.; Sun, B.; Imai, H.; Mimoto, T.; Kondoh, K. Powder metallurgy titanium metal matrix composites reinforced with carbon nanotubes and graphite. *Compos. Part A* **2013**, *48*, 57–66. [[CrossRef](#)]
22. Lascoste, E.; Arvieu, C.; Quenisset, J.M. Correlation between microstructures of SiC reinforced titanium matrix composite and liquid route processing parameters. *J. Mater. Sci.* **2015**, *50*, 5583–5592. [[CrossRef](#)]
23. Liu, J.; Wu, M.X.; Yang, Y.; Yang, G.; Yan, H.X.; Jiang, K. Preparation and mechanical performance of graphene platelet reinforced titanium nanocomposites for high temperature applications. *J. Alloys Compd.* **2018**, *765*, 1111–1118. [[CrossRef](#)]
24. Mu, X.N.; Zhang, H.M.; Cai, H.N.; Fan, Q.B.; Zhang, Z.H.; Wu, Y.; Fu, Z.J.; Yu, D.H. Microstructure evolution and superior tensile properties of low content graphene nanoplatelets reinforced pure Ti matrix composites. *Mater. Sci. Eng. A* **2017**, *687*, 164–174. [[CrossRef](#)]
25. Mu, X.N.; Cai, H.N.; Zhang, H.M.; Fan, Q.B.; Zhang, Z.H.; Wu, Y.; Ge, Y.X.; Wang, D.D. Interface evolution and superior tensile properties of multi-layer graphene reinforced pure Ti matrix composite. *Mater. Des.* **2018**, *140*, 431–441. [[CrossRef](#)]

26. Zhou, H.T.; Su, Y.J.; Liu, N.; Kong, F.T.; Wang, X.P.; Zhang, X.; Chen, Y.Y. Modification of microstructure and properties of Ti-47Al-2Cr-4Nb-0.3W alloys fabricated by SPS with trace multilayer graphene addition. *Mater. Charact.* **2018**, *138*, 1–10. [[CrossRef](#)]
27. Dong, L.L.; Lu, J.W.; Fu, Y.Q.; Huo, W.T.; Liu, Y.; Li, D.D.; Zhang, Y.S. Carbonaceous nanomaterial reinforced Ti-6Al-4V matrix composites: Properties, interfacial structures and strengthening mechanisms. *Carbon* **2020**, *164*, 272–286. [[CrossRef](#)]
28. Antunes, E.F.; Lobo, A.O.; Corat, E.J.; Trava-Airoldi, V.J.; Martin, A.A.; Verissimo, C. Comparative study of first-and second-order Raman spectra of MWCNT at visible and infrared laser excitation. *Carbon* **2006**, *44*, 2202–2211. [[CrossRef](#)]
29. Mu, X.N.; Cai, H.N.; Zhang, H.M.; Fan, Q.B.; Wang, F.C.; Zhang, Z.H.; Wu, Y.; Ge, Y.X.; Chang, S.; Shi, R.; et al. Uniform dispersion of multi-layer graphene reinforced pure titanium matrix composites via flake powder metallurgy. *Mater. Sci. Eng. A* **2018**, *725*, 541–548. [[CrossRef](#)]
30. Yan, S.J.; Dai, S.L.; Zhang, X.Y.; Yang, C.; Hong, Q.H.; Chen, J.Z.; Lin, Z.M. Investigating aluminum alloy reinforced by graphene nanoflakes. *Mater. Sci. Eng. A* **2014**, *612*, 440–444. [[CrossRef](#)]
31. Xiong, D.B.; Cao, M.; Guo, Q.; Tan, Z.Q.; Fan, G.L.; Li, Z.Q.; Zhang, D. Graphene-and-Copper Artificial Nacre Fabricated by a Preform Impregnation Process: Bioinspired Strategy for Strengthening-Toughening of Metal Matrix Composite. *ACS Nano* **2015**, *9*, 6934–6943. [[CrossRef](#)]
32. Bánhegyi, G. Comparison of electrical mixture rules for composites. *Colloid Polym. Sci.* **1986**, *264*, 1030–1050. [[CrossRef](#)]
33. Kim, H.S. On the rule of mixtures for the hardness of particle reinforced composites. *Mater. Sci. Eng. A* **2000**, *289*, 30–33. [[CrossRef](#)]
34. Nairn, J.A. On the use of shear-lag methods for analysis of stress transfer in unidirectional composites. *Mech. Mater.* **1997**, *26*, 63–80. [[CrossRef](#)]
35. Boostani, A.F.; Yazdani, S.; Mousavian, R.T.; Tahamtan, S.; Khosroshahi, R.A.; Wei, D.; Brabazon, D.; Xu, J.Z.; Zhang, X.M.; Jiang, Z.Y. Strengthening mechanisms of graphene sheets in aluminum matrix nanocomposites. *Mater. Des.* **2015**, *88*, 983–989. [[CrossRef](#)]
36. Yilmaz, S.; Dunand, D.C. Finite-element analysis of thermal expansion and thermal mismatch stresses in a Cu-60vol%ZrWO composite. *Compos. Sci. Technol.* **2004**, *64*, 1895–1898. [[CrossRef](#)]
37. Sinev, L.S.; Ryabov, V.T. Reducing thermal mismatch stress in anodically bonded silicon-glass wafers: Theoretical estimation. *J. Micro/Nanolithography MEMS MOEMS* **2017**, *16*, 015003. [[CrossRef](#)]
38. Zhang, Z.; Chen, D.L. Contribution of Orowan strengthening effect in particulate-reinforced metal matrix nanocomposites. *Mater. Sci. Eng. A* **2008**, *483*, 148–152. [[CrossRef](#)]
39. Kombaiyah, B.; Murty, K.L. Coble Orowan Strengthening, and Dislocation Climb Mechanisms in a Nb-Modified Zircaloy Cladding. *Metall. Mater. Trans. A* **2015**, *46*, 4646–4660. [[CrossRef](#)]
40. Asgharzadeh, H.; Simchi, A.; Kim, H.S. Microstructure and Mechanical Properties of Oxide-Dispersion Strengthened Al6063 Alloy with Ultra-Fine Grain Structure. *Metall. Mater. Trans. A* **2011**, *42*, 816–824. [[CrossRef](#)]
41. Morris, M.A. Deformation mechanisms in fine-grained Ti-Al alloys. *Mater. Sci. Eng. A* **1997**, *224*, 12–20. [[CrossRef](#)]
42. Bai, M.W.; Namus, R.; Xu, Y.D. Inkson, In-situ Ti-6Al-4V/TiC composites synthesized by reactive spark plasma sintering: Processing, microstructure, and dry sliding wear behaviour. *Wear* **2019**, *432–433*, 20–29.
43. Arsenault, R.J.; Shi, N. Dislocation generation due to differences between the coefficients of thermal expansion. *Mater. Sci. Eng.* **1986**, *81*, 175–187. [[CrossRef](#)]

